

# ASCA Observations of the Twin Supernova Remnants in the Large Magellanic Cloud, DEM L316

Mamiko NISHIUCHI, Jun YOKOGAWA and Katsuji KOYAMA\*

*Department of Physics, Graduate School of Science, Kyoto University, Sakyo-ku, Kyoto, 606-8502*

*E-mail(MN): mamiko@cr.scphys.kyoto-u.ac.jp*

and

John P. HUGHES†

*Department of Physics and Astronomy, Rutgers University, 136 Frelinghuysen Road, Piscataway, NJ 08854-8019*

(Received ; accepted )

## Abstract

We report results from an ASCA X-ray study of DEM L316, an emission nebula in the Large Magellanic Cloud (LMC) consisting of two closely-spaced supernova remnants (SNRs). The SIS image shows separate X-ray sources located at the positions of the two radio- and optically-emitting SNR shells, 0547–69.7A and 0547–69.7B (hereafter, shell A and B). The individual X-ray spectrum of each shell is well described by optically-thin thermal emission, although the characteristics of the emission differ in important details between them. Shell A exhibits strong iron L emission, which we attribute to the presence of iron-rich ejecta leading to the suggestion that this SNR originates from a Type Ia SN, an explosion of a moderate mass progenitor. Shell B, on the other hand, has a chemical composition similar to that of the interstellar medium of the LMC and so its X-ray emission is dominated by swept-up matter. The different spectral features strongly disfavor the hypothesis that the two shells are due to one supernova explosion into an interconnected bubble. We could not obtain the evidence which positively supports the collision between two SNRs.

**Key words:** SNR: individual (DEM L316) — galaxies: individual (LMC) — interstellar matter — X-rays: SNRs

## 1. Introduction

Nuclear burning in stars and their subsequent explosions as supernovae (SNe) are the primary means by which heavy elements are synthesized and distributed in the interstellar medium (ISM) of galaxies. The chemical composition of SN ejecta depends strongly on the type of the SN explosion and the mass of the progenitor. For example, type Ia SNe, which produce iron-rich ejecta, are believed to be the incineration of a CO white dwarf driven to the Chandrasekar limit by accretion (Nomoto, Thielemann, & Yokoi 1984). A type II (or Ib/c) SN, the core-collapse of a massive star, tends to eject large amounts of oxygen produced during the hydrostatic evolution of the progenitor (Tsujimoto et al. 1995). The mix of SNe types, plus the nucleosynthetic yield of individual SNe, is an essential element that determines the chemical evolution of galaxies and the structure and dynamics of the ISM. SNe often produce remnants (SNRs) containing

hot ( $10^7$  K) X-ray emitting plasma with spectra characterized by numerous emission lines from heavy elements. X-ray spectroscopy therefore provides a powerful tool for determining the chemical composition of SN ejecta and the ambient medium, as well as the amount of energy input to the ISM.

The radio SNR DEM L316 is located in the nearest sizeable galaxy, the Large Magellanic Cloud (LMC), at a distance of  $\sim 50$  kpc (van den Bergh 2000). The LMC's nearly face-on geometry, or small inclination angle ( $30^\circ - 40^\circ$ ; Feast 1991), and its location at high Galactic latitude result in only modest interstellar absorption for individual objects in the Cloud. Thus, unlike most Galactic SNRs, DEM L316 has a reliable distance estimate and low ISM absorption. DEM L316 consists of a pair of closely-spaced, limb-brightened shells of radio and optical emission, called SNR 0547–69.7A and SNR 0547–69.7B (hereafter shell A and shell B). It has been proposed that these twin shells are (1) two independent remnants superposed along the line of sight (Mathewson and Clarke 1973), (2) a single SN that exploded into an interconnected bubble formed by a stellar wind or a previous supernova (Lasker 1981; Mills et al. 1984), or (3) “col-

\* CREST, Japan Science and Technology Corporation (JST), 4-1-8 Honmachi, Kawaguchi, Saitama, 332-0012

† also Service d'Astrophysique, L'Orme des Merisiers, CEA Saclay, 91191 Gif-sur-Yvette Cedex FRANCE

liding remnants” (Williams et al. 1997). Because of the similarity in their mean radial velocities, some authors (Lasker 1981; Williams et al. 1997) have argued that the two shells are physically co-located. In fact the individual mean radial velocities of the two shells are only poorly constrained, largely because they each come from averaging over the complex velocity field of an incomplete SNR shell expanding at a velocity of  $\sim 200 \text{ km s}^{-1}$  (Williams et al. 1997). Unfortunately Williams et al. (1997) do not assess quantitatively the level of difference in mean velocity of the two shells allowed by their data. These authors also found enhanced [O III] emission and a change in the magnetic field structure in the region between shell A and B, from which they inferred that the two shells in DEM L316 were indeed colliding SNRs.

Our recent study of LMC SNRs (Hughes, Hayashi, & Koyama 1998) has shown that ASCA X-ray spectra can provide powerful constraints on the nature, evolution, and composition of remnants. As part of our continuing research effort in this area we undertook ASCA observations of DEM L316. The current article presents our detailed X-ray spectral study of each shell using nonequilibrium ionization models. We find that the ASCA data do indeed provide important insights into the nature of DEM L316 and shed light on the relationship between shells A and B.

## 2. Observations and Data Reduction

ASCA observed DEM L316 on 27 August, 1999. X-rays were focused by the four XRTs (X-ray Telescopes) separately onto two GIS (Gas Imaging Spectrometer) and two SIS (Solid-state Imaging Spectrometer) detectors. The instruments are sensitive in the energy bands 0.7–10 keV (GIS) and 0.4–10 keV (SIS). The GIS and SIS were operated in PH mode and 1-CCD faint mode, respectively. The roll angle of the observaion was adjusted so that at the position of DEM L316 the stray light from LMC X-1 was blocked by the mirror support housing. Details of the ASCA telescope and detectors are presented in Serlemitsos et al. (1995), Ohashi et al. (1996) and Burke et al. (1994).

The X-ray data were first screened with the usual criteria: data obtained during South Atlantic Anomaly passages, with a cut-off rigidity lower than  $4 \text{ GeV c}^{-1}$ , or with an elevation angle to the limb of the Earth less than  $5^\circ$  were rejected. For the GIS, rise-time information was used to further reject non-X-ray events. For the SIS, we also rejected events obtained when the elevation angle to the limb of the bright Earth was smaller than  $25^\circ$  and with a cut-off rigidity lower than  $4 \text{ GeV c}^{-1}$ . Hot and flickering pixels were removed and only standard event grades 0, 2, 3, and 4 were used. The net exposure time after screening was  $6.0 \times 10^4 \text{ s}$  (SIS) and  $5.6 \times 10^4 \text{ s}$  (GIS). The increase in the charge-transfer-inefficiency of

the SIS CCDs over the course of the ASCA mission has resulted in a number of deleterious effects including degraded spectral resolution and a decrease in the detection efficiency for X-ray photons (due to grade migration and on-board event rejection). We therefore applied the RDD (Residual Dark Distribution) correction as described by Dotani et al. (1997) to recover some of the lost spectral resolution. This results in an energy resolution for the SIS of  $\sim 7\%$  (FWHM) at 1 keV. The decrease in X-ray photon detection efficiency is incorporated into the response function of the SIS.

We also extracted spectra from ROSAT PSPC (Position Sensitive Proportional Counter) archival data (sequence number 500259) originally observed in October 1993 for 4.0 ks. The PSPC was sensitive over the energy range 0.1–2.4 keV and had an energy resolution at 1 keV of  $\sim 43\%$  (FWHM). The on-axis angular resolution of the PSPC was  $13''$  (50% encircled energy radius) (Pfeffermann et al. 1987), which was sufficient to cleanly separate the X-ray emission from the two shells in DEM L316.

## 3. Analyses and Results

### 3.1. SIS and PSPC X-ray Spectra

In Figure 1 we show the ASCA SIS image in two energy bands; the soft (0.4–1.2 keV) and hard (1.2–7.0 keV) X-ray band images are shown as the grayscale and contour map, respectively. We see X-ray emission from both radio shells A and B. Since the half-power diameter of the ASCA XRT ( $\sim 3'$ ) is comparable to the angular separation between the shells ( $\sim 2.5'$ ), the SIS data do not cleanly resolve the two SNRs and therefore each shell is contaminated by X-rays that spill-over from the other shell. In order to minimize this spill-over effect and take advantage of the sharp core of the ASCA XRT point-spread-function, we carefully selected the source and background regions. The source regions, as shown in Figure 2a, were rather small ellipses with major axes of  $1'$  centered on the peak emission from each shell. The background regions were the same size as the source regions, were situated beyond the remnant, and were located so that the source and background regions for one shell were roughly the same distance from the source region of the other shell. We note that the overall ASCA SIS fluxes are not well determined since only a portion of each shell was included in the small spectral extraction regions used. In order to obtain a more accurate estimate of the overall flux of each shell and to provide stronger constraints on the soft X-ray absorption toward the SNR, we thus extracted ROSAT PSPC spectra using the source and background regions shown in Figure 2b. Clearly the emission from shells A and B is cleanly separated in the PSPC data.

The SIS and PSPC spectra were simultaneously fitted to an optically-thin thermal plasma spectral model. All spectral parameters were linked between the data sets for a given shell with the exception of the SIS and PSPC normalization factors which were each allowed to vary freely. Below we present results based on the nonequilibrium ionization (NEI) spectral code by Masai (1994) (hereafter referred to as the Masai model) although, as a cross check, the NEI model of Hughes & Singh (1994) was also used to verify results. In general there was good agreement between the two NEI spectral calculations and in particular we find roughly the same best-fit elemental abundances. The specific NEI model employed was the single-timescale, single-temperature model, which parameterizes the NEI condition through a quantity called the ionization timescale ( $n_e t_i$ ). Here  $n_e$  and  $t_i$  are the mean electron density and elapsed time after the plasma was heated to the temperature  $kT$ . The equilibrium ionization condition is attained for values of  $n_e t_i > 10^{12} \text{ cm}^{-3} \text{ s}$ . In the following we refer to this as collisional ionization equilibrium (CIE).

### 3.1.1. Shell A

In our NEI fits to the data of shell A, we first allowed the temperature, column density and ionization parameter to be free, while the abundances of all the elements were fixed to be 0.3 times solar, the average in the LMC (see Russell & Dopita 1992, Hughes et al. 1998). This model, however, was statistically unacceptable (the  $\chi^2$  of 85.4 for 52 degrees of freedom can be rejected at the 99.7% confidence level), and furthermore the data showed an excess of emission relative to the model around 1 keV. This energy band contains the L-shell lines of iron and the  $K\alpha$  lines of neon, which raises the interesting possibility that one or both of these species may be relatively overabundant in shell A.

In order to test this hypothesis we tried several model fits including cases with (1) only the neon abundance free, (2) only the iron abundance free, and (3) both the iron and neon abundances free. In these fits the column density to shell A was fixed to  $N_H = 3.8 \times 10^{21} \text{ cm}^{-2}$ , a value that is consistent with our preliminary fits (described in the preceding paragraph) and an independent estimate from the HI column to the SNR (Williams et al. 1997). The abundances of the other elemental species were fixed to be 0.3 times solar, as above. Model 1 was rejected since it was unable to account for the excess residual emission between 1 to 2 keV, while Models 2 and 3 were both acceptable from a statistical point of view. In the two latter cases, the iron abundance was found to be significantly higher than the LMC mean value. However, a similar statement about the abundance of neon in shell A could not be made, since the neon abundance determined in model 3 was not well constrained. In ta-

ble 1 we present the best-fit parameters from our case 2 model fits. Figure 3a shows the spectral data, best-fit model spectrum and residuals. The best-fit value of the iron abundance is  $1.9_{-0.6}^{+0.9}$  times solar, a factor of 5 more than the mean LMC value, which clearly indicates a large overabundance of iron in shell A. We also note that the ionization timescale range allows for the possibility that the X-ray-emitting plasma is in CIE, as shown in the two-dimensional  $\chi^2$  contours of  $kT$  vs.  $n_e t_i$  (Figure 4a).

### 3.1.2. Shell B

For this shell the NEI model with fixed LMC mean abundances (0.3 solar) provided an acceptable fit to the spectrum. As before the best-fit column was fixed to the value  $N_H = 3.8 \times 10^{21} \text{ cm}^{-2}$ . The  $\chi^2$  confidence contours between ionization timescale and temperature are shown in Figure 4b. This plot indicates that we could not constrain whether the plasma in shell B is in NEI or CIE condition because the confidence level for rejecting the CIE model is slightly low (68%), though the best fit ionization timescale favors the NEI case. Therefore, we also carried out the spectral fitting for the CIE case. The best fit parameters for both the NEI and CIE case are in Table 1. Figure 3b shows plots of the data, model, and residuals only for the NEI case, because the best-fit spectrum in CIE is almost the same as that in NEI.

### 3.1.3. X-ray spectra with GIS

The spatial resolution of the GIS is somewhat poorer than that of the SIS, which makes separating the X-ray emission from the two shells in DEM L316 nearly impossible. Thus we made a composite GIS spectrum containing the total emission from shells A and B again summing data from both detectors. We fit this GIS spectrum using the the best fit SIS/PSPC spectral parameters and found the fit to be acceptable, thereby establishing consistency between the GIS and SIS/PSPC data.

## 4. Discussion

The main difference between the spectral characteristics of shell A and B is the strong emission line structure at about 1 keV seen in the spectrum of shell A. Our spectral analysis of shell A suggests an enhanced iron abundance. It is well known that Type Ia SNe are efficient producers of iron (Nomoto, Thielemann, & Yokoi 1984), while massive-star core-collapse SNe tend to produce proportionally more of the lower atomic number species, such as oxygen, neon, and magnesium (Tsuji-moto et al. 1995). Therefore one might argue that the emission line structure around 1 keV may be described by a combination of  $K\alpha$  lines from oxygen and neon, which are major elements yielded by type II SNe, rather than L shell lines from iron. To check this possibility,

we further treated the abundances of neon, oxygen, and iron as free parameters and fitted the shell A spectra to the NEI model. Then we found that the abundance of iron was again significantly higher than the mean LMC value. However, a similar statement about the abundances of oxygen and neon could not be made, since the abundances of both of these elements were not well constrained. At least one other middle-aged LMC SNR (DEM 71) shows evidence for enhanced iron in its global integrated ASCA spectrum (Hughes et al. 1998). We, therefore, believe that the enhanced iron in shell A is strong evidence in support of the origin of shell A as a Type Ia SN.

Assuming that the electron and ion densities in the plasma are identical, that the X-ray emitting plasma has uniform density and that the distance to DEM L316 ( $D$ ) is 50 kpc, we can estimate the ion density ( $n_i$ ) in both shells through

$$n_i = 1.7N_{12}^{0.5}(V/10^{59}\text{cm}^3)^{-0.5}(D/50\text{kpc})\text{cm}^{-3}, \quad (1)$$

where  $N_{12}$  is the emission measure derived from the spectral fits (in units of  $10^{12}\text{cm}^{-5}$ ) and  $V$  is the volume of the X-ray emitting plasma (in units of  $\text{cm}^3$ ).

We estimate the volume using the ROSAT HRI morphology (Williams et al. 1997) as follows. For shell A, we assume that the plasma fills a spherical region with a radius of 11 pc. Because shell B has limb-brightened morphology, we tentatively assumed that the Sedov model applies to shell B, i.e., the thickness of shell B is one twelfth of the shell radius (shell radius was assumed to be 15 pc, Williams et al. 1997).

From equation (1), we obtain values of  $\sim 0.4\text{cm}^{-3}$  for the ion density of the plasma in shell A. Adopting this density and the best-fit ionization parameter  $n_e t_i$ , we derive an ionization timescale age for shell A of  $\sim 3.9 \times 10^4$  yr.

For shell B, the spectral fitting gives two local minimums for the NEI conditions of  $n_e t_i \sim 10^{10.7}$  (case 1) and  $n_e t_i \sim 10^{12}$  (case 2). Depending on these two cases, we obtain different physical parameters, particularly for the ionization age. In case 1, the plasma density is  $\sim 0.5$ , for which case the ionization parameter ( $n_e t_i$ ) gives an age ( $t_i$ ) of  $\sim 3.2 \times 10^3$  yr. However, in case 2, the plasma density is  $\sim 0.8$  and the age is estimated to be  $> 4.2 \times 10^4$  yr (the CIE condition is attained for values of  $n_e t_i > 10^{12}$ ). Shell B is larger and has lower surface brightness than shell A, which suggest that shell B is the older of the two. We thus infer that the evidence favors case 2, which places shell B at an older age ( $> 4.2 \times 10^4$  yr) than that found for shell A above.

Finally we propose, from the totally different spectral shapes of shell A and B, that these two shells were not due to a single supernova explosion into a pre-existing bubble made by a stellar wind or an SN. We also propose, from

the iron over abundance seen in the spectrum, that the origin of shell A is a Type Ia.

## 5. Summary

The first detailed spectral analysis of DEM L316 was demonstrated with the ASCA satellite. The spectra of shell A exhibited strong L-shell lines of iron, thus we conclude that shell A has Type Ia SN origin. On the other hand, the shell B spectra was well reproduced with the thin-thermal plasma model whose abundance was similar to that of the interstellar medium of the LMC. These totally different spectral characteristics strongly contradict the hypothesis that two shells were due to a single supernova explosion into a pre-existing bubble made by a stellar wind or an SN. We could not obtain the evidence which positively supports the collision between two SNRs nor could we get a strong constraint for the shell B progenitor. To further investigate these problems more spatially sensitive observations in X-ray band will be needed, such as with the Chandra satellite.

JPH extends his thanks to Monique Arnaud for her support and hospitality during the course of this project. Partial funding was also provided by NASA grant NAG5-6420 to Rutgers University. We thank Marc Gagné for his contributions to the initial planning of these observations. This research has made use of data obtained from the High Energy Astrophysics Science Archive Research Center (HEASARC), provided by NASA's Goddard Space Flight Center. MN and JY are financially supported by JSPS Research Fellowship for Young Scientists.

## References

- Burke B.E., Mountain R.W., Harrison D.C., Bautz M.W., Doty J.P., Ricker G.R., Daniels P.J. 1991, IEEE Trans. ED-38, 1069
- Dotani T., Yamashita A., Ezuka H., Takahashi K., Crew G., Mukai K., the SIS team 1997, ASCA news 5, 14
- Feast M.W. 1991, in IAU Symp. 148, The Magellanic Clouds, ed. R.Haynes & D.Milne (Dordrecht : Kluwer), 1
- Hughes J.P., Hayashi I., Koyama K. 1998, ApJ 505, 732
- Hughes J.P., Singh K.P. 1994, ApJ 422, 126
- Lasker B.M. 1981, PASP 93, 422
- Mathewson D.S., Clarke J.N. 1973, ApJ 180, 725
- Mills B.Y., Turtle A.J., Little A.G., Durdin J.M. 1984, Australian J. Phys. 37, 321
- Nomoto, K., Thielemann, F.-K., Yokoi, M. 1984, ApJ 286, 644
- Ohashi T., Ebisawa K., Fukazawa Y., Hiyoshi K., Horii M., Ikebe Y., Ikeda H., Inoue H. et al. 1996, PASJ 48, 157
- Pfeffermann E., Briel U.G., Hippmann H., Kettenring G., Metzger G., Predehl P., Reger G., Stephan K.H. et al. 1987, Proc. SPIE 733,519

Table. 1 Fitting results.

	Shell A	Shell B (CIE)	shell B (NEI)
$N_{\text{H}}$ ( $10^{21}$ cm $^{-2}$ )	3.8 <sup>†</sup>	3.8 <sup>†</sup>	3.8 <sup>†</sup>
$kT_e$ (keV)	0.90 (0.86–1.09)	0.72 (0.68–0.76)	1.13 (0.87–1.52)
$\log n_e t_i$ (cm $^{-3}$ s)	11.74 (11.07–13.00)	13.00 <sup>†</sup>	10.73 (10.53–11.07)
Fe *	1.9 (1.3–2.8)	0.3 <sup>†</sup>	0.3 <sup>†</sup>
Other species †	0.3 <sup>†</sup>	0.3 <sup>†</sup>	0.3 <sup>†</sup>
EM <sup>‡</sup> ( $10^{10}$ cm $^{-5}$ )	6.9 (3.7–7.0)	16.6 (14.6–18.6)	8.4 (7.0–10.1)
$\chi^2$ (d.o.f)	50.9 (52)	46.1 (45)	43.4 (44)

Parentheses indicate 90% confidence intervals for a single relevant parameter ( $\Delta\chi^2 = 1$ )

<sup>†</sup> Fixed parameter

\* Abundance of iron relative to the solar value.

† Abundances of other elements relative to their solar values.

<sup>‡</sup> Emission measure, defined as:  $(n_i^2 V)/(4 \pi D^2)$ . See text for details.

Russell S.C., Dopita M.A. 1992, ApJ 384, 508

Serlemitsos P.J., Jalota L., Soong Y., Kunieda H., Tawara Y.,  
Tsusaka Y., Suzuki H., Sakima Y. et al. 1995, PASJ 47,  
105

Tsujimoto T., Nomoto K., Yoshii Y., Hashimoto M.,  
Yanagida S., Thielemann F.K. 1995, MNRAS 277, 945

van den Bergh, S. 2000, PASP 112, 529

Williams R.M., Chu Y.H., Dickel J.R., Beyer R., Petre R.,  
Smith R.C., Milne D.K. 1997, ApJ 480, 618

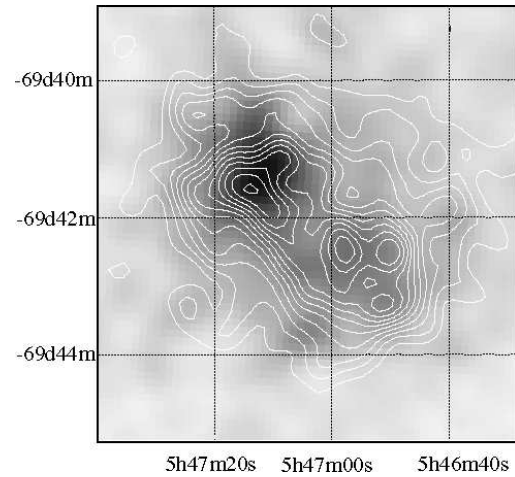


Fig. 1.. ASCA SIS image of DEM L316 (SNR 0547–69.7) after summing both detectors and smoothing with a gaussian filter of  $\sigma = 15''$ . The grayscale and contours represent the 0.4–1.2 keV and 1.2–7.0 keV bands, respectively. Contours are linearly spaced in steps of  $2.8 \times 10^{-4}$  cts s $^{-1}$  arcmin $^{-2}$  and sky coordinates are epoch J2000. The two X-ray sources correspond to shell A (northeastern source) and shell B (southwestern source), respectively.

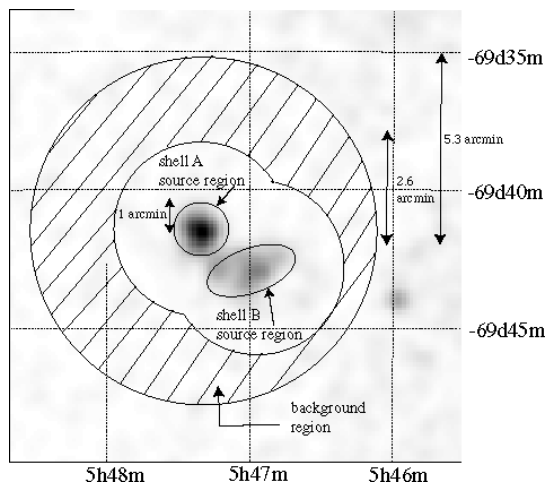
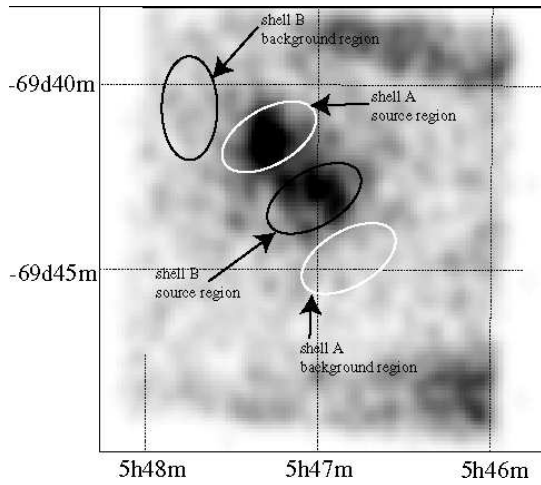


Fig. 2.. The source and background regions (see text) overlaid on the ASCA SIS (a) and ROSAT PSPC (b) total band images.

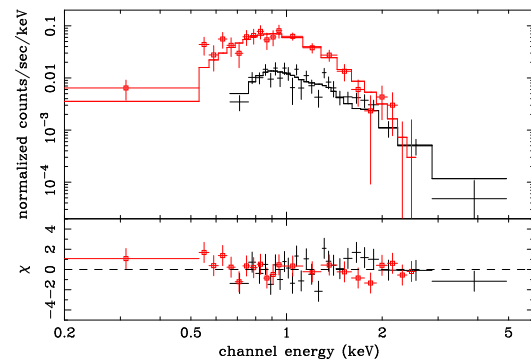
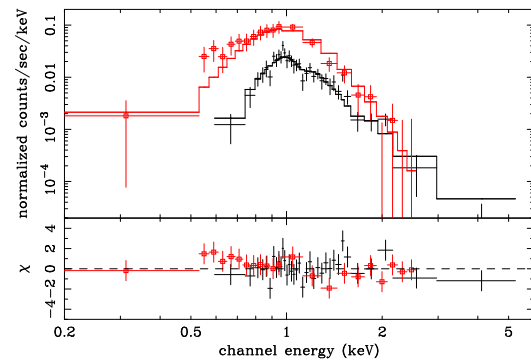


Fig. 3.. X-ray spectra of shell A (a) and shell B (b) from the ASCA SIS (crosses) and ROSAT PSPC (boxes). The top panels show the data and best-fit models, while the lower panels shown the residuals. Errors are purely statistical at  $1\sigma$  confidence. The spectra appear to differ the most around 1 keV. We attribute the more sharply peaked emission from shell A near 1 keV to enhanced iron L line emission (see text for details).

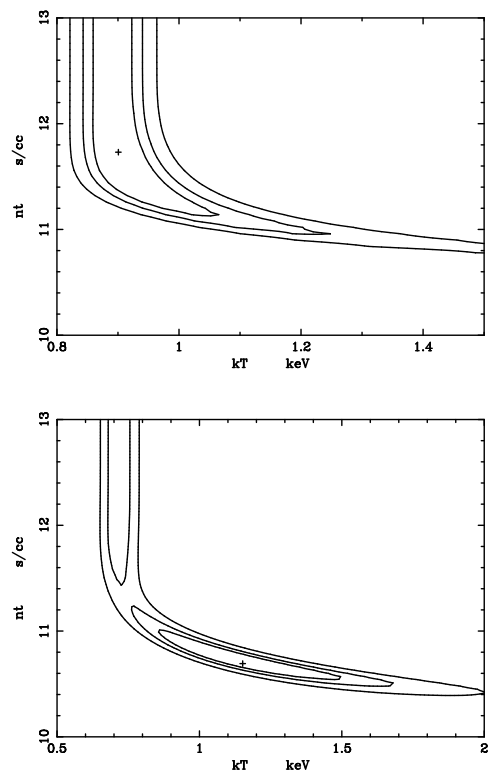


Fig. 4.. Confidence contours between fitted electron temperature ( $kT$ ) and ionization timescale ( $nt$ ) for shell A (a) and shell B (b). Contours are shown at the 68%, 90% and 99% confidence levels. The best-fit parameters are indicated by crosses.